Environ Fluid Mech (2013) 13:279–307
DOI 10.1007/s10652-013-9274-7

ORIGINAL ARTICLE

Flow and turbulence in an industrial/suburban roughness canopy

A. Dallman · S. Di Sabatino · H. J. S. Fernando

Received: 12 September 2012 / Accepted: 6 February 2013 / Published online: 7 March 2013

Abstract A field study conducted to investigate the flow and turbulence structure of the urban boundary layer (UBL) over an industrial/suburban area is described. The emphasis was on morning and evening transition periods, but some measurements covered the entire diurnal cycle. The data analysis incorporated the dependence of wind direction on morphometric parameters of the urban canopy. The measurements of heat and momentum fluxes showed the possibility of a constant flux layer above the height $z \approx 2H$, wherein the Monin-Obukhov Similarity Theory (MOST) is valid; here H is the averaged building height. For the nocturnal boundary layer, the mean velocity and temperature profiles obeyed classical MOST scaling up to $\sim 0.5\Lambda$ ($\sim 6H$), where Λ is the Obukhov length scale, beyond which stronger stratification may disrupt the occurrence of constant fluxes. For unstable and neutral cases, MOST scaling described the mean data well up to the maximum measured height ($\sim 6H$). Available MOST functions, however, could not describe the measured turbulence structure, indicating the influence of additional governing parameters. Alternative turbulence parameterizations were tested, and some were found to perform well. Calculation of integral length scales for convective and neutral cases allowed a phenomenological description of eddy characteristics within and above the urban canopy layer. The development of a significant nocturnal surface inversion occurred only on certain days, for which a criterion was proposed. The nocturnal UBL exhibited length scale relationships consistent with the evening collapse of the convective boundary layer and maintenance of buoyancy-affected turbulence overnight. The length

A. Dallman (✉) · S. Di Sabatino · H. J. S. Fernando
Environmental Fluid Dynamics Laboratories, Department of Civil and Environmental Engineering and Earth Sciences, University of Notre Dame, Notre Dame, IN 46556, USA
e-mail: ardallm@gmail.com

S. Di Sabatino
Laboratorio di Micrometeorologia, Dipartimento di Scienze e Tecnologie Biologiche ed Ambientali, Università del Salento, Lecce, Italy

H. J. S. Fernando
Department of Aerospace and Mechanical Engineering, University of Notre Dame, Notre Dame, IN 46556, USA

and velocity scales so identified are useful in parameterizing turbulent dispersion coefficients in different diurnal phases of the UBL.

Keywords Urban effects · Turbulence scales · Thermal stratification · Nocturnal boundary layer · Morphometric analyses

1 Introduction

With urban areas now accounting for more than 50 % of where the world population lives [1], and continued rapid urbanization at a rate of 1.5 % per year, much recent focus has been placed on understanding and managing of an urban metabolism—which deals with the flow of material, heat, air and water; infrastructure; utilization of resources; environmental change, and human and social dynamics [2,3]. Of critical importance in such studies is the lowest atmospheric layer affected by the ground, known as the urban boundary layer (UBL), which hosts a variety of ecosystems, including human activities. This is the layer through which exchanges of heat, momentum, species and moisture between the ground surface and atmosphere take place, which in turn determine the microclimate, dispersion of pollutants/contaminants and hydrologic cycle. Given its complexity, the UBL is studied by invoking processes occurring over a repertoire of scales, and interactions therein determine the nature and evolution of the UBL. For example, the properties averaged over a suitable urban footprint from a 'bird's eye view' may provide a large ($\gtrsim$ meso) scale perspective. In regulatory enforcement, representative microcosms within a large urban area (e.g., pollutant or temperature hot-spots) are defined by 'neighborhood' scales [4]. An area encompassing a cluster of downtown buildings is used in emergency [5,6] and city planning [7]. The flow in a single urban street canyon is used for evaluating pedestrian comfort [8,9].

The UBL is divided into several vertically stacked layers, each selected on the basis of dynamical characteristics and having specific length and time scales [10–12]. The layer up to the roof heights, the urban canopy layer (UCL), develops between roughness elements, wherein the flow is highly inhomogeneous, dependent on local urban morphometry and sensitive to small-scale features within urban canyons. The roughness sub-layer (RSL) extends from the ground up to about two to five times the height of roughness elements (i.e., building height H). Within the RSL the flow is three-dimensional, turbulence is inhomogeneous and vertical diffusion is as important as horizontal advection. Upward expanding wakes of individual buildings are felt in this layer, and due to the merging of wakes, the role of individual buildings disappears upwards. The inertial sub-layer or constant flux layer (CFL) is above the RSL, in which the signatures of individual building wakes and upstream conditions are absent and turbulence is determined by the 'averaged' building morphology. A (perhaps misleadingly called) mixed layer (ML) with varying shear stresses tops the CFL, and extends upwards to the edge of the UBL where transition to free stream (with geostrophic flow U_G) is completed, the ground influence is lost and entrainment of free-stream air is a key feature.

Naturally, the parameterization of flow and turbulence in the UCL and RSL is a difficult challenge, given their dependence on the details of the underlying urban surface. On the other hand, given the perceived horizontal homogeneity and nearly constant upward turbulent fluxes, Monin-Obukhov similarity theory (MOST) has been applied to the CFL, but the bane has been acquiring measurements within the CFL [8] to verify the applicability of MOST. On physical grounds, MOST functions are expected to depend on the urban roughness. Very little information is available on the ML.

A substantial amount of meteorological measurements have been reported in urban areas, including large experimental programs with hundreds of investigators, observations across multiple scales and with the deployment of extensive instrumentation. Some examples are URBAN 2000 [13], Joint Urban 2003 [14], DAPPLE [15], UBL/CLU-ESCOMPTE [16], and BUBBLE [17]. There are also many studies conducted by smaller groups of investigators dealing with specific problems [8]. Informative review material on past work can be found in Roth [11], Britter and Hanna [8], and Wood et al. [18]. The parameterization of turbulence in the UBL has been a topic of much interest, given its importance in modeling the fate of airborne releases and local air pollution. Most studies have been focused on the CFL, considering the prospects of universal parameterizations based on MOST. By considering horizontally homogeneous turbulence in the CFL determined by the momentum flux or the friction velocity u_* and the bulk integral scale ℓ of turbulence at its lower boundary, a dimensional analysis approach can be attempted to identify key parameters. Any property P can thus be written as

$$P = P\left[u_*, \ell, (z-d), q_o, h_u\right], \tag{1}$$

where $q_o = g\overline{w'\theta'}/\theta_0$ is the buoyancy flux (with g being the acceleration of gravity, θ_0 the reference potential temperature, and $\overline{w'\theta'}$ the flux of temperature), h_u the height of the UBL, z the distance from the ground, and d the displacement height that accounts for the virtual origin from which the distances are measured for the CFL, $z' = (z-d)$. Note that d and ℓ are functions of the aerodynamic roughness height (z_0) of the underlying surface. The non-dimensional form of Eq. 1 is

$$P^* = P^*[z'/\Lambda, \ell/\Lambda, \ell/h_u] \tag{2}$$

where $\Lambda = -u_*^3/\kappa q_0$ is the Obukhov length scale and $\zeta = z'/\Lambda$ is a stability parameter. For $\ell/h_u \ll 1$, assuming that eddies of size $\sim h_u$ do not penetrate the CFL, self-similarity of the first kind [19] yields,

$$P^* = P_1^*\left[z'/\Lambda, \ell/\Lambda\right]. \tag{3a}$$

On the other hand, when the influence of eddies of size $\sim h_u$ are present, self-similarity of the second kind may produce

$$P^* = \left(\frac{\ell}{h_u}\right)^m P_2^*\left[\frac{z'}{\Lambda}, \frac{\ell}{\Lambda\,(\ell/h_u)^n}\right], \tag{3b}$$

where m and n are unknown exponents. Similarly, for the neutral case ($\Lambda \to \infty$),

$$P^* = P_3^*\left[z'/\ell\right], \tag{4a}$$

or

$$P^* = \left(\frac{\ell}{h_u}\right)^{m_1} P_4^*\left[\frac{z'}{\ell}\left(\frac{\ell}{h_u}\right)^{n_1}\right], \tag{4b}$$

where ℓ can be replaced by the independent length scale at the top of the RSL, z_0. Although general equations for the UBL are given by Eq. 3(a,b), it has been customary to use the form

$$P^* = G^*\left[z'/\Lambda\right], \tag{5}$$

[11], and naturally, the function G^* is expected to depend on ℓ/Λ and ℓ/h_u (or h_u/Λ), that is on the site and the thermal stratification [20]. The observance of varying functions and the scatter of data in previous studies, at least partly, can be attributed to this dependence.

Table 1 shows various forms of G^* for root mean square (rms) velocities ($\sigma_i, i = u, v, w$) and the rms temperature (σ_T), where $T_* = -\overline{w'\theta'}/u_*$, for stable ($\zeta > 0$) and unstable ($\zeta < 0$) atmospheric conditions noted in previous studies (and for current data). Alternative parameterizations are also available for specific cases. Involvement of a large number of parameters clearly adds to the difficulty of UBL analysis.

Another unexplored issue is the formation of a stable layer near the ground at night [12,27]. In dense urban canopies, wakes of obstructions cause strong mechanical mixing, which, when augmented by the urban heat island (UHI), can overshadow the stabilizing influence of cooling [28,29]. Measurements in London [18] and Rome [30], however, show that near surface stable stratification may occur in large urban areas rather frequently.

While previous field [11], laboratory [31,32] and numerical [33] studies have made significant advances, substantial knowledge gaps exist on flow and turbulence in urban canopies. Some of the overarching issues are:

- Is there a CFL and is it horizontally homogeneous? What are the velocity and temperature profiles in various layers of the UBL?
- Can MOST work well over urban areas, and what are its limitations?
- Are the varying MOST functions at different locations a result of z_0 and h_u dependence?
- How do available alternative (to MOST) turbulence parameterizations perform for the UBL?
- When a stably stratified flow approaches a roughness canopy, how do the competing effects of mechanical turbulence and buoyancy sway the structure of the UBL?
- Can a stably stratified boundary layer develop near the surface of built up areas? What is its structure and what are the scales of turbulence?
- What is the scale of the UBL under different stability conditions, and what is the role of the so-called ML in effacing the ground effects at greater heights?

The data from a field study conducted in the Hermoso Park neighborhood of Southwest Phoenix during Nov/Dec 2009 were employed to address the above questions. The site is made up of mixed urban-industrial land use, and heightened health problems of local residents were a driving factor of the field study. It has been argued that anomalous airborne particulate matter (PM) concentration in the area, both due to local re-entrainment and transport from elsewhere, may be responsible for the health woes. This PM is further contaminated by small concentrations of lead particles in the soil, deposited from past (1991, 2000) fires at two local circuit board manufacturing facilities. Since PM is re-entrained by turbulence, flow and surface turbulence in the area (as well as in urban canopies in general) were of prime interest, and are the theme of this paper.

Phoenix is located in complex terrain, and hence, is characterized by up-valley (daytime) and down-valley (nighttime) winds [2,34]. Two towers were used, each instrumented with three sonic anemometers, and depending on the wind direction and stability conditions, they were representative of different layers of the UBL. Because of the non-uniformity of the urban area, the urban morphological parameters used in the analysis were different for different approach directions of wind. Measurements were recorded over the diurnal cycle, with tethered balloon launches in the early evening (1400–2000 LST) and morning (0500–1100 LST) whence the PM concentrations are highest due to weak flow during evening/morning transition periods.

The detailed experimental procedure is given in Sect. 2, including the evaluation of morphometric parameters. Sections 3.1 and 3.2 present overall diurnal meteorological and turbulence fields over a selected design period, which characterize the overall experiment. Section 3.3 deals with the measurement of turbulence, focusing on the parameterization of

Table 1 Various forms of Eq. 5 suggested by previous studies and the current data (adapted from Wood et al. [21])

Reference	σ_u/u_*	σ_v/u_*	σ_w/u_*	σ_T/T_*	Comments
Panofsky et al. [22]	$(12-0.5\zeta)^{1/3}$	$(12-0.5\zeta)^{1/3}$	$1.3\,(1-3\zeta)^{1/3}$	n/a	Unstable
Roth [11]	$1.98\,(1-0.33\zeta)^{0.56}$	$1.64\,(1-2.84\zeta)^{0.30}$	$1.12\,(1-2.48\zeta)^{0.33}$	$-3.03\,(1-24.4\zeta)^{-0.33}$	Unstable, urban review
	$1.88\,(1-0.15\zeta)^{0.94}$	$1.52\,(1-3.34\zeta)^{0.31}$	$1.15\,(1-2.09\zeta)^{0.33}$	$-4.10\,(1-65\zeta)^{-0.33}$	Unstable, urban review, only for z/H > 2.5
Pahlow et al. [23]	$2.3+4.3\zeta^{0.5}$	$2.0+4.0\zeta^{0.6}$	$1.1+0.9\zeta^{0.6}$	$0.05\zeta^{-1}+3$	Stable
Moraes et al. [24]	$2.4\,(1-3.4\zeta)^{0.31}$	$2.2\,(1-4.4\zeta)^{0.33}$	$1.2\,(1-5.3\zeta)^{0.33}$	n/a	Unstable
	$2.4\,(1+106\zeta)^{0.1}$	$2.2\,(1+300\zeta)^{0.1}$	$1.2\,(1+4.3\zeta)^{0.33}$	n/a	Stable
Wilson [25]	n/a	n/a	$1.25\,(1-3\zeta)^{1/3}$	n/a	Unstable
Quan and Hu [26]	$1.96\,(1+2.07\zeta)^{1/3}$	$1.80\,(1+1.78\zeta)^{1/3}$	$1.42\,(1+0.54\zeta)^{1/3}$	$3.0\,(\zeta)^{-1/3}$	Stable
	$2.03\,(1-0.50\zeta)^{1/3}$	$1.70\,(1-1.05\zeta)^{1/3}$	$1.33\,(1-1.27\zeta)^{1/3}$	$-1.5\,(-\zeta)^{-1/3}$	Unstable
Wood et al. [21]	$2.23\,(1-0.22\zeta)^{1/3}$	$1.78\,(1-0.57\zeta)^{1/3}$	$1.31\,(1-0.65\zeta)^{1/3}$	$-1.4\zeta^{-1/3}$	Unstable
	$2.36\,(1+1.15\zeta)^{0.20}$	$1.92\,(1+1.33\zeta)^{0.22}$	$1.40\,(1+0.46\zeta)^{0.19}$	$3.41\zeta^{-0.18}$	Stable
Current data	$1.81\,(1-5.26\zeta)^{1/3}$	$1.39\,(1-15.5\zeta)^{1/3}$	$0.98\,(1-5.64\zeta)^{1/3}$	$-3.4\,(1-21\zeta)^{-1/3}$	Unstable
	$2.95\,(1+1.91\zeta)^{1/3}$	$2.35\,(1+3.00\zeta)^{1/3}$	$1.35\,(1+0.55\zeta)^{1/3}$	$2.6\,(\zeta)^{-1/3}$	Stable

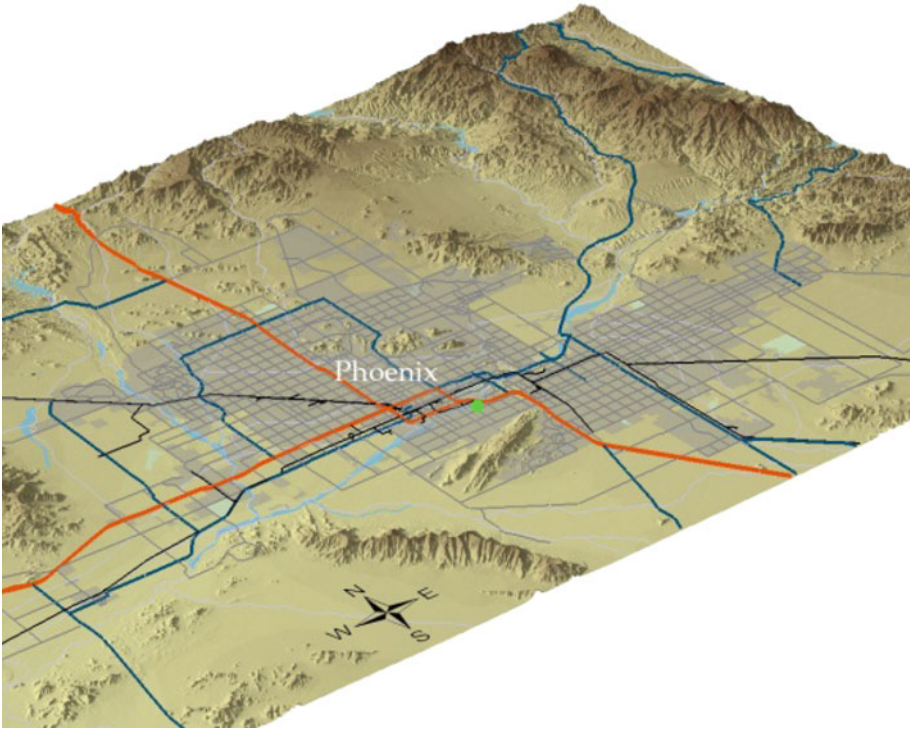

Fig. 1 Topography surrounding the Phoenix area, with high terrain to the east. The *green dot* indicates the locality of the Hermoso Park neighborhood

rms velocities and length scales. Section 3.4 discusses the conditions for the generation of stratification in the lower UBL, the length scales of the UBL and those used in stably stratified turbulence studies, and estimates of the stable UBL height. The paper concludes with a summary of findings in Sect. 4.

2 Experimental design and site characteristics

2.1 Experimental setup

Figure 1 shows a view of the Phoenix area confined by surrounding mountain ranges, with high mountains to the east dominating the thermal circulation. The Hermoso Park neighborhood, the area of interest, is enlarged in Fig. 2, showing the details of building morphometry. The study area was sanctioned by the State of Arizona, in need of information on air pollution and dispersion for decision making. The observation sites included the Southwest Airlines Reservation Center (designated by 'SWA') parking lot (2320 E Jones St, Phoenix; 33°24′41″ N, 112°01′54″ W) and HD Supply Waterworks (3622 S 30th St, Phoenix; 33°24′51″ N, 112°01′04″ W) designated by 'HD'. The two sites were separated by $\approx$ 1.5 km. In the absence of synoptic influence, the nocturnal (down-valley) flow is easterly and the daytime (up-valley) flow is westerly [2].

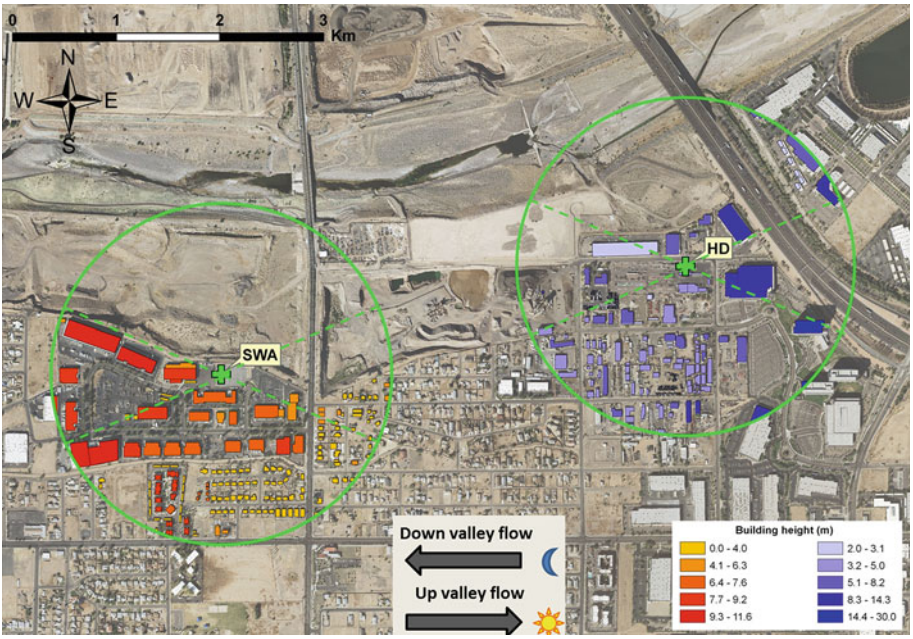

Fig. 2 The morphometry of the study area, with building heights indicated in the lower right hand corner. Up- and down-valley flow directions are also shown

2.1.1 SWA site

At this site, a tethered balloon, a SODAR/RASS and a 14-m meteorological tower were deployed. A 9 m^3 Väisälä tethered balloon, equipped with a meteorological tethersonde TTS111, was used for vertical profiling of air temperature (resolution 0.1°C), relative humidity (1 %), atmospheric pressure (0.1 hPa), wind speed (0.1 ms^{-1}) and wind direction (1°) from the ground up to 60 m, a limit set by Federal Aviation Administration air traffic control because of the proximity of the site to the Phoenix Sky Harbor Airport. Vertical profiles were measured every 10 min from ∼ 0500 LST to 1100 LST to capture the morning transition, and from ∼ 1400 LST to 2000 LST to observe the evening transition.

A Scintec MFAS SODAR acoustic wind profiler, installed with a RAE-1 radio acoustic sounding system (RASS) extension for temperature profiles, was used for measurements from 50 m upward (resolution ∼ 15 m), the maximum height being determined by instrument noise. Mounted on the 14-m tower were two temperature and relative humidity probes (Campbell Scientific CS500) at 6.8 and 12.1 m above the ground level (agl), sampled at 5 Hz, and a net radiometer [Kipp & Zonen CNR1, sensitivity 5–18 μV $(Wm^{-2})^{-1}$, response time 18 s, accuracy ± 10 %] located at 10.1 m agl. The radiometer measured the incoming/outgoing short wave radiation and incoming/outgoing long wave radiation at 5 Hz, from which the net radiation could be calculated. Three 3D sonic anemometers (R.M. Young 81000) were placed at 2.9, 10.2 and 14.7 m agl to measure the u, v, w velocities (resolution and accuracy: 0.01 and ±0.05 ms^{-1}) and virtual air temperature, T_v (resolution and accuracy: 0.01 and ±2°C) at 20 Hz. A Campbell Scientific CR5000 data logger stored all tower data at the site.

2.1.2 HD site

This site also had a 14-m tower with two thermistors and relative humidity sensors mounted at 6.9 and 12.2 m agl, and three sonic anemometers (Campbell Scientific CSAT3; R.M. Young 81000) at 3.0, 10.3 and 14.6 m. All data were stored in a CR3000 data logger. Also placed at a nearby location was a Väisälä CL31 ceilometer, which can detect multiple cloud layers in the atmosphere up to several kilometers. The height of the convective boundary layer could be estimated by post-processing of data using standard algorithms provided with the instrument.

2.2 Morphological parameters

Given the locational dependence of Eq. 5, a detailed investigation of site morphology was required prior to any flow analyses. The morphology analysis provided, with an adequate degree of accuracy for full-scale conditions, relevant parameters required for interpreting the results. The study area varied from bare land with sparse urban development directly north of each site to a residential and industrial neighborhood to the south of the sites, with the fully-developed urban settlement of the city of Phoenix located a few kilometers northwest. For the analysis, the study area was subdivided into two main sectors, considering that surface roughness characteristics approaching from the west and east are different. Using three-dimensional digital building data, known as urban digital elevation models (DEMs), the methodology described in Di Sabatino et al. [35] was used to calculate relevant flow parameters.

The methodology consists of two parts: direct building data analysis and calculation of synthetic morphometric parameters using MATLAB based algorithms. Urban DEMs, typically produced in a CAD© format, are transformed into a gray-scale image (raster format) in which each pixel has a color value that is proportional to the building height. Image processing techniques are then used to calculate the morphometric parameters (see Ratti et al. [36] for a review), namely the effective building height H, frontal area density λ_f and planar area density λ_p; these were used to estimate z_0 and d. Two different DEMs, each encompassing a set of buildings surrounding a site, were analyzed separately for the two main flow directions of interest ($270 \pm 22.5°$ for westerly winds and $90 \pm 22.5°$ for easterly winds). The radii for the sites were selected to be greater than the adjustment length scale (Sect. 2.3). The $\pm 22.5°$ arcs used for the calculations of H, λ_f, and λ_p are shown in Fig. 2, and z_0 and d were estimated using the formulae of Macdonald et al. [37]:

$$\frac{d}{H} = 1 + \left(\lambda_p - 1\right) \alpha^{-\lambda_p} \tag{6}$$

$$\frac{z_0}{H} = \left[1 - \frac{d}{H}\right] exp\left\{-\left[\frac{0.5 \beta C_D \lambda_f}{\kappa^2}\left(1 - \frac{d}{H}\right)\right]^{-0.5}\right\}, \tag{7}$$

with $\alpha = 4.43$, $\beta = 1.0$, $\kappa = 0.4$ (the von Karman constant), and drag coefficient $C_D \sim 1$. This methodology is known to give better estimates than other geometric-based parameterizations [38]. Table 2 reports building statistics and related morphometric parameters for the two sites, based on two wind directions.

Table 2 suggests that the roughness canopy in point is rather sparse. According to the specifications of Grimmond and Oke [39], z_0/H and d/H, as functions of λ_p and λ_f, in general fall in the category of *suburban areas*. Accordingly, for westerly flow, both sites are in the wake interference regime, and for easterly flow both are in the isolated roughness regime. Although z_0/H and d/H are calculated from λ_p and λ_f rather than profile mea-

Table 2 Morphological parameters calculated based on DEM analyses

	Westerly flow (daytime)	Easterly flow (nighttime)
SWA site		
$H(m)$	9.62	4.61
λ_f	0.05	0.02
λ_p	0.23	0.05
$d(m)$	4.33	0.52
$z_0(m)$	0.18	0.03
z_0/H	0.02	0.01
d/H	0.45	0.11
HD site		
$H(m)$	3.54	13.13
λ_f	0.03	0.02
λ_p	0.19	0.09
$d(m)$	1.37	2.77
$z_0(m)$	0.04	0.14
z_0/H	0.01	0.01
d/H	0.39	0.21

surements, the ratios obtained are broadly consistent with Britter and Hanna [8], where for $\lambda_f < 0.15$, $z_0/H = \lambda_f$ and $d/H = a_0\lambda_f$, with $a_0 = 3$ for large planar area densities λ_p. For the present data, $a_0 = 10$, which may account for the smaller λ_p of the sites.

2.3 Adjustment length scale

The distance required for the flow to reach equilibrium upon change of surface roughness (e.g., encountering an urban area) can be evaluated as [40]

$$L_c = \frac{2\,(1-\beta_s)\,H}{C_D\lambda_f}, \tag{8}$$

where β_s is the solid fraction of the buildings. Using the characteristic values $C_D = 1$, $\beta_s \approx \lambda_p$ (sparse), the adjustment lengths for westerly and easterly flows are 300 and 440 m for SWA and 190 and 1,200 m for HD, respectively. Therefore, the locations of the measurement sites are considered as representative of the neighborhood, given that flows arriving at the sites are fully adjusted to local morphological features.

3 Results

3.1 General observations

The generic local flow behavior at the two sites was investigated based on 20 min averages of sonic data at the same level. The averaging period was selected based on several factors: the nonstationary nature of turbulence during transition periods, averaging periods greater than the integral time scales [41], and the timescales of forcing variability. Figure 3 shows averaged mean flow U, wind direction, air temperature T, sensible heat flux $Q_h = \rho C_p \overline{w'\theta'}$, where

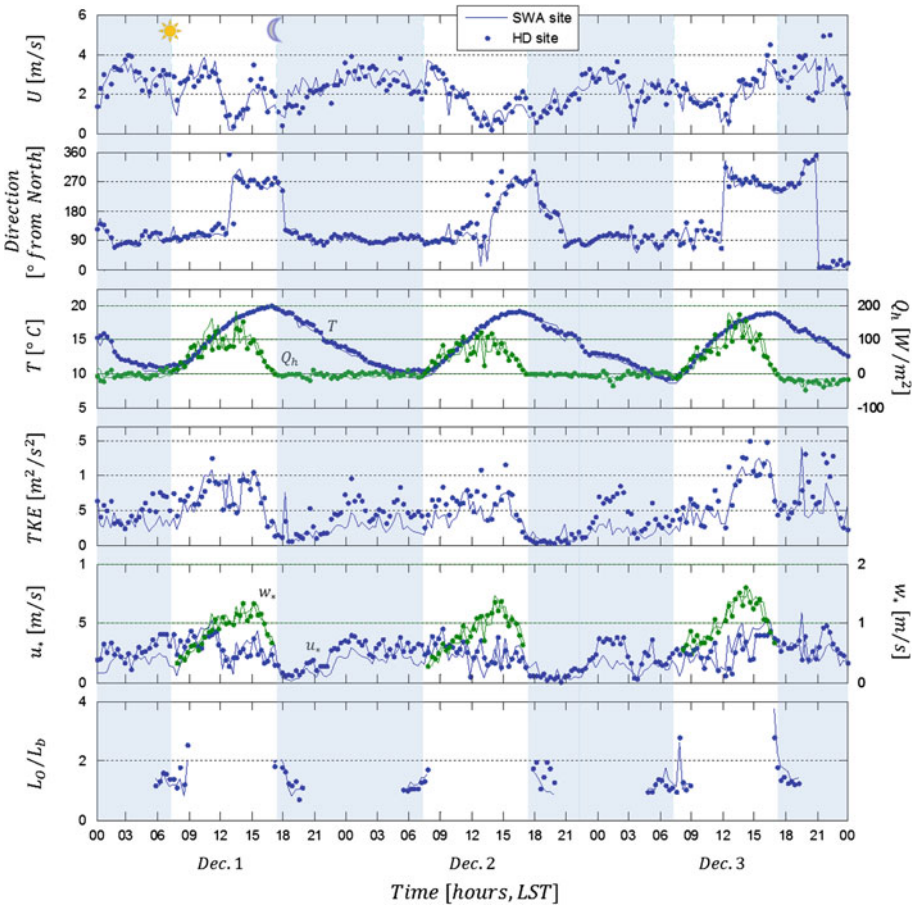

Fig. 3 Twenty minute averaged meteorological and fluid dynamics relevant variables for each site on Dec 1–3, 2009 based on measurements at 14.7 m (SWA site) and 14.6 m (HD site). Balloon data were also used for calculation of L_O/L_b, see the text for details

ρ is the density and C_p the specific heat of air; turbulent kinetic energy (TKE); convective velocity scale $w_* = \left(q_o h_u^c\right)^{1/3}$ (where h_u^c is the boundary layer height during convective periods); friction velocity $u_* = \left[\left(\overline{u'w'}\right)^2 + \left(\overline{v'w'}\right)^2\right]^{1/2}$; and the ratio of the Ozmidov and buoyancy length scales L_O/L_b (see Sect. 3.4) based on measurements at 14.7 and 14.6 m for the SWA and HD sites, respectively. The three design days were selected based on the dominance of local thermal circulation, as evident from repeated diurnal patterns of up-valley (westerly) and down-valley (easterly) flows (i.e., low synoptic activity). In general, both sites recorded similar mean flow, wind direction, air temperature and sensible heat flux characteristics, except for some isolated strong fluctuations that could be attributed to local wind gusts. The TKE at the HD site was noticeably high, especially during the night, probably due to high roughness (0.14 vs. 0.03 m at SWA; Table 2) encountered by the nocturnal flow; associated intense turbulence is also reflected from higher u_* values. At night, because of the stable stratification of approach flow to the urban canopy, the difference in u_* is reflected

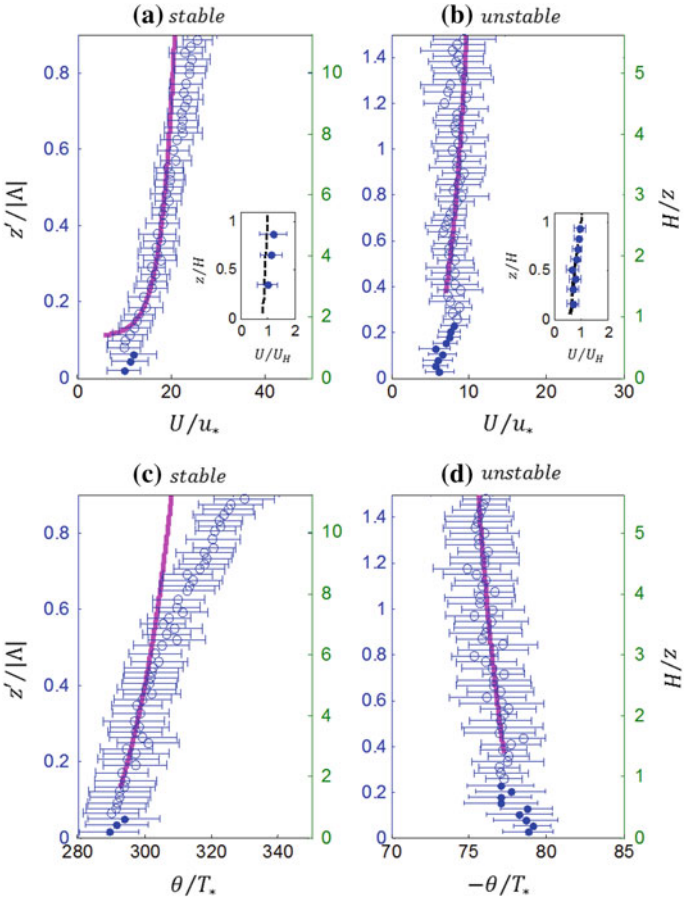

Fig. 4 Non-dimensional averaged velocity and temperature profiles during **a**, **c** stable, and **b**, **d** unstable periods for the SWA site, where *filled* and *open circles* represent measurements within and above the UCL, respectively. The *inset* shows the same measurements with different scaling variables for comparisons with the UCL formulation in Eq. 10. The *error bars* represent one standard deviation from the mean

only mildly on the mean flow, given that vertical propagation of momentum fluxes is impeded by stable stratification. Then the mean flow is mostly determined by pressure gradients and averaged surface shear stresses, and detailed stress distribution in the UBL plays a lesser role in determining the mesoscale flow.

The w_* values at both sites are approximately the same, a reflection of similar heat fluxes. The evening transition usually occurs about a half to 1 h after the heat flux becomes negative, but when the daytime heat flux and upslope flow velocities are high or the cooling flux and stable stratification is stronger, it can be delayed by up to three hours (e.g., Dec 3), a phenomenon that has been attributed to the inertia of the upslope flow and its disconnection from the stable near-surface layer [42]. When the evening transition is sharp, it is associated with a brief increase of turbulence levels (Dec 1, 3), due to formation of a transition front, as described by Hunt et al. [43]. Even after transition, sporadic increases of turbulence are possible due to arrival of intrusive fronts from different directions [44,45]. The morning transition in all cases occurred toward midday.

3.2 Mean velocity and temperature profiles

The balloon data were used to obtain vertical profiles of mean velocity U and potential temperature θ for stable (a, c) and unstable (b, d) periods at the SWA site (Fig. 4). The profiles were selected from Dec 1, 2 and 3, and were categorized into 'stability classes' according to the background averaged Brunt–Väisälä (buoyancy) frequency $N^2 = (g/\theta_0)(\partial\theta/\partial z)$ between 30 and 50 m. For $N^2 > 0.001\text{s}^{-2}$ the flow was considered stable, for $N^2 < -0.001\text{s}^{-2}$ unstable, and for $-0.001\text{s}^{-2} < N^2 < 0.001\text{s}^{-2}$ neutral. For both nocturnal and daytime periods, this N^2 corresponded to that of the CFL ($z/H > 2$), and therefore is not directly affected by surface inhomogeneity. Figure 4 displays an average of individual profiles for each stability class, plotted as a function of the non-dimensional effective height $z'/|\Lambda|$ based on the balloon data. The scaling parameter Λ was selected to illustrate the regions of different dynamical characteristics (e.g., shear dominated at $z < \Lambda$ and buoyancy dominated for $z > \Lambda$) and to validate MOST. The right ordinate shows an alternative normalization z/H. The error bars refer to one standard deviation from the mean values. The friction velocity u_* and the temperature scale T_* were calculated based on the 14.7 m sonic, which is representative of CFL. For completeness, Fig. 5 shows a vertically extended plot (up to $\sim$ 150 m agl) to illustrate the consistency of SODAR/RASS and tethered balloon profiles.

Shown in Fig. 4 are the vertical profiles predicted by MOST, which is strictly valid in the CFL $z \gtrsim 2H$ (see Sect. 3.3.1). We have used the canonical profiles [46],

$$u(z) = \frac{u_*}{\kappa} ln\left(\frac{z'}{z_0}\right) \tag{9a}$$

for neutral,

$$u(z) = \frac{u_*}{\kappa}\left[ln\left(\frac{z'}{z_0}\right) - 5\frac{z}{\Lambda}\right] \tag{9b}$$

for stable, and

$$u(z) = \frac{u_*}{\kappa}\left[ln\left(\frac{z'}{z_0}\right) - \psi_m\right] \tag{9c}$$

for unstable cases, where ψ_m is the integral of $\left(1-(1+16|\zeta|)^{-1/4}\right)/\zeta$. During stable periods (Fig. 4a, c), the data accord with Eq. 9b well up to $\sim \Lambda/2$ ($2H \lesssim z \lesssim 6H$) and clearly deviate for $z' \gtrsim 0.6|\Lambda|$, where z_0 and d are from Table 2.

In the stable boundary layer, mechanical turbulence dominates to a height on the order Λ, and this limiting height may be identified as $\Sigma \approx (0.5-0.6)\Lambda$. For $z > \Sigma$, the flow is buoyancy dominated, including strong internal waves (see the lidar observations of Wang et al. [47] for the SBL over Oklahoma City). This aspect can be further studied by calculating relevant length scales of stratified turbulence, such as the Ozmidov $[L_0 = \left(\varepsilon/N^3\right)^{1/2}]$ and buoyancy $[L_b = \sigma_w/N]$ length scales; here ε is the rate of dissipation of turbulent kinetic energy and σ_w is the vertical rms velocity. They represent the vertical scale where the buoyancy starts strongly influencing turbulence [48]. According to laboratory studies [49,50], the vertical scale of a fully turbulent region generated mechanically in a backdrop of stable stratification and shear, analogous to the lower UBL, is given by $h_p \approx 3L_b$ (and this scaling also holds true even for shear-free turbulence [51]). Beyond this height, turbulence is strongly damped by buoyancy effects, essentially disconnecting different horizontal layers stacked up vertically. Ensuing failure of MOST can be estimated by inspecting profiles of Fig. 4, and this occurs at a height $z'/\Lambda \sim 0.6$ which corresponds to $z \sim 30$ m, consistent with $L_b \approx 10$ m.

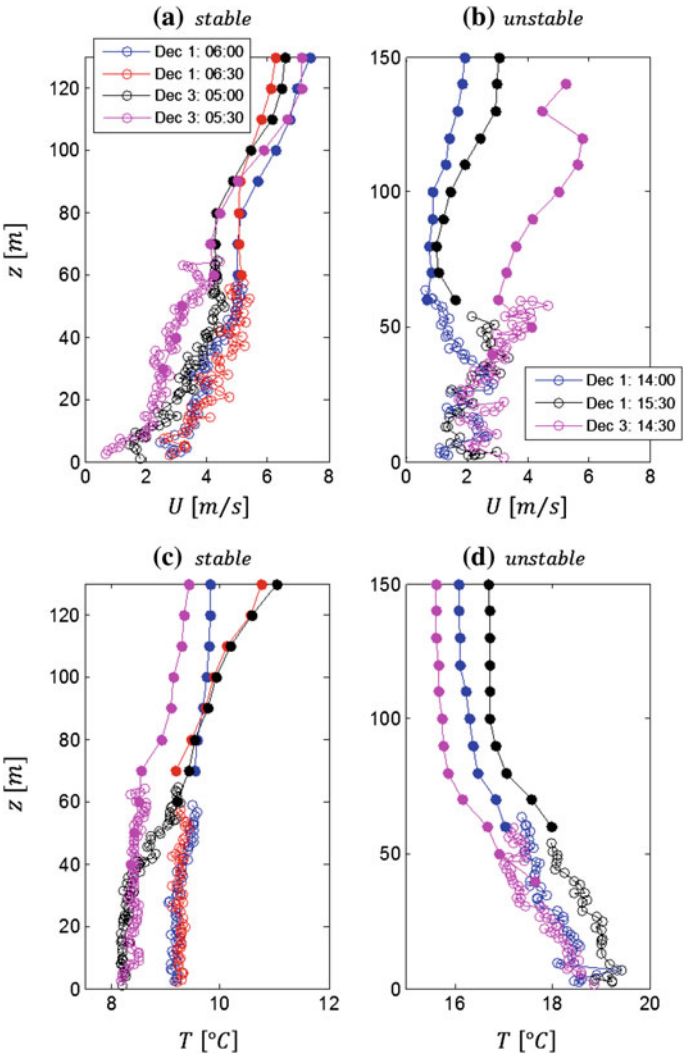

Fig. 5 Individual velocity and temperature profiles (single realizations) during stable and unstable periods at the SWA site. *Filled circles* are sodar data, and *open circles* are from the tethered balloon

Beyond $3L_b$ the fluxes are damped by stratification, and u_* is not a suitable scale (also see Sect. 3.4).

Conversely, in the convective regime, ground information first propagates upward by mechanical and then by convective turbulence. Hence, MOST is expected to be valid over much larger vertical extents ($\gtrsim$ 60m), as evident from Fig. 4b, d.

Neutral conditions last only for a short duration, usually during transition periods. Corresponding data from the morning transition with prevalent downslope flow is shown in Fig. 6, with Eq. 9c fitted over $2 < z/H < 11$. The existence of a logarithmic layer is indicated, which allows calculation of profile-based roughness height $z_{0p} \approx 0.12$ m, which is about four times that computed via DEM ($z_0 \approx 0.03$m). Note that z_0 calculated from the DEM

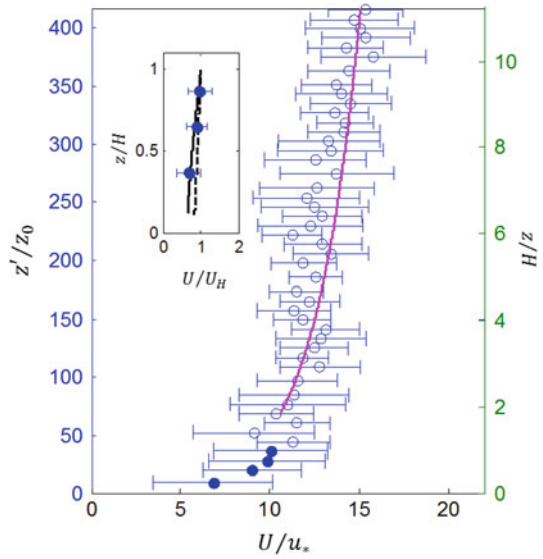

Fig. 6 Same as Fig. 4, but during neutral periods for the SWA site

considered buildings in the sector 90° ± 22.5°, but additional features such as trees and larger buildings outside the sector may increase the roughness, which may partly account for the disparity. SODAR data (not shown) displayed deviations from the logarithmic profiles beyond $z \approx 18H$, which can be considered as the top of the CFL for the neutral case.

Obviously MOST is inapplicable in the UCL, and to this end Macdonald [31] has extended the mixing length formulation of Cionco [52] developed for plant canopies to urban canopies. For lower packing densities, $\lambda_f < 0.35$, it was proposed

$$U(z) = U_H \, exp\left[a\left(z/H - 1\right)\right], \tag{10}$$

where z is the vertical height from the ground and U_H the mean velocity at $z = H$. For a simple cubicle array, Macdonald proposed $a = a_M = 9.6\lambda_f$. While only a few data points are available, Eq. 10 could be evaluated for the UCL using balloon data, and the resulting velocity profiles with a selected from the best fit to the data are shown in the insets of Fig. 4.

For stable cases, the actual velocity profiles are almost linear with $\alpha \ll 1$, compared to $a_M = 9.6\lambda_f = 0.19$. This deviation is not unexpected because stable stratification tends to decouple lower air layers from the ground, thus making z dependence weaker and causing assumptions underlying Eq. 10, such as constant mixing length, invalid. Low Reynolds stresses at $z < H$ support this argument (Fig. 7). Interestingly, subdued friction causes mean velocity in the UCL to be slightly higher than that in the RSL. In all, Eq. 10 is not suitable for the stable UCL of sparse urban canopies.

Encouraging results were found for the convective case where Eq. 10 has better applicability; $a = 0.55$ (Fig. 4b), which is in good agreement with $a_M = 9.6\lambda_f = 0.48$. For the neutral case (Fig. 6), the best fit $a = 0.5$ compared only modestly with the calculated $a_M = 0.9$. Recalling that Macdonald's [31] formula was obtained for cubicle obstacles, this disparity is not unexpected. Overall, the use of Eq. 10 for practical applications for convective and neutral cases is broadly supported by our data.

In engineering practice, for example in wind power generation or dispersion calculations, the mean profiles in the UBL are approximated by a power law (e.g., Karlsson [53], Macdonald [31]),

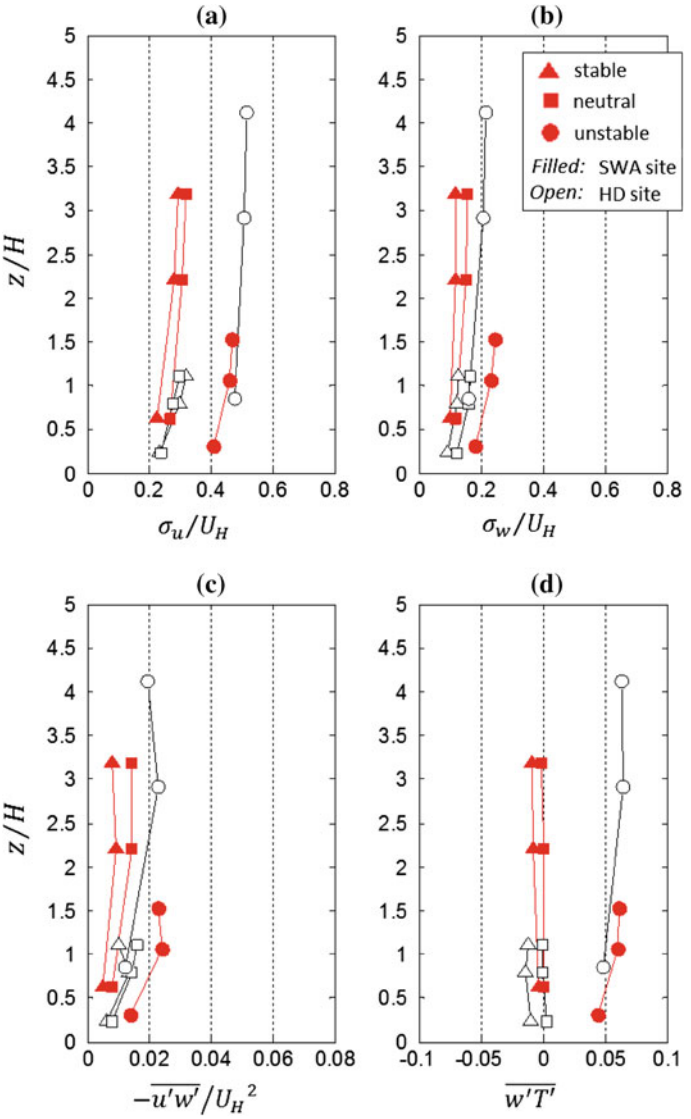

Fig. 7 Averaged turbulent intensity and flux profiles derived from the sonic anemometers at SWA site (*filled symbols*) and HD site (*open symbols*) during stable (*triangle*), neutral (*square*), and unstable (*circle*) periods

$$\frac{U(z)}{U_H} = \left(\frac{z}{H}\right)^p, \tag{11}$$

where p is a power law index that depends on the atmospheric stability [54]. Macdonald [31] fit laboratory data for $z \gtrsim 2H$ and obtained $p = 0.26$ for the neutral case. For the present data taken at $z > 2H$, $p = 0.15$ for the neutral case, $p = 0.07$ for the unstable case, and $p = 0.39$ for the stable case. This accords with Pérez et al. [54], who found $p < 0.2$ for daytime, but slightly differs from their nocturnal case where $p \gtrsim 0.5$.

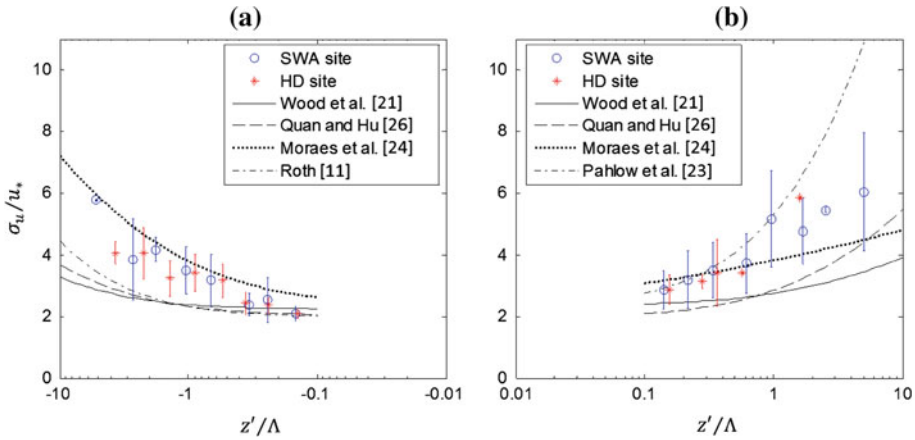

Fig. 8 Thirty minute averages of the normalized characteristic rms velocity versus stability parameter z'/Λ. Only the upper sonic from each site is shown

3.3 Turbulence

3.3.1 Variance of turbulent velocities and turbulent fluxes

Figure 7a, b shows the measured normalized rms horizontal (σ_u) and vertical (σ_w) velocities as a function of the dimensionless height. The fluxes of momentum and heat are shown in Fig. 7c, d. In each case, the normalized rms velocities do not appear to change substantially with height for $z/H > 1$, but their magnitudes depend on the stability regime (recall that H depends on the site and flow direction; Table 2). Larger λ_p and λ_f values for SWA and HD for westerly flow, augmented by convection, give higher rms velocities during the daytime. In the stable and neutral regimes, rms values tend to be smaller, in part due to low λ_p and λ_f.

The Reynolds stress and heat flux distributions are noteworthy, which tend to be constant for $z > 2H$ for all cases, although more data would have helped arriving at more definitive conclusions (here the heat flux is not scaled, given the misleadingly small normalized values). This suggests a CFL amenable for MOST formulation. Thus, for profiles in Fig. 4, we have used fluxes measured by the top sonic for MOST evaluations, but at times, depending on H, the achievable z/H did not extend to the CFL.

Previous studies in Washington DC and New York City have shown that, in the skimming flow regime, turbulent intensities within the UCL are low, given the lack of penetration of mean flow into the UCL [55]. In contrast, the building canopy in the present case is sparse and belongs to the isolated roughness/wake interference regime, and the turbulent flow aloft communicates well with the UCL, thus elevating turbulence levels in the latter. The vertical distribution of turbulent intensities is further discussed below in the context of MOST and other parameterizations.

3.3.2 Applicability of MOST

For comparison with MOST, the u-component of *rms* velocity data, σ_u, from the topmost sonics were divided into 30-min segments and then bin averaged. The data for different stability classes were selected as follows: unstable when $\zeta \leq -0.1$, stable when $\zeta \geq 0.1$. In the data presented, the approach velocity to the canopy is $\geq$2 m/s. The MOST functions

Table 3 Turbulence parameterizations

Authors	Parameterization	Conditions
Hanna and Britter [56]	$\sigma_u/u_* = 2.4$; $\sigma_v/u_* = 1.9$; $\sigma_w/u_* = 1.3$	Neutral
André et al. [57]	$\sigma_A = \left(1.75u_*^2 + w_*^2\right)^{1/2}$	Convective
Deardorff [58]	$\sigma_D = \left(w_*^3 + \eta^3 u_*^3\right)^{1/3}$, $\eta = 1.8$	Convective
Clarke et al. [59]	$\sigma_C = C_u \left(w_*^3 + u_*^3 \lambda_{max}/(\kappa z)\right)^{1/3}$, $C_u \approx 0.4 - 0.6$	Convective, λ_{max} is the energy containing wave length

derived are given in Table 1 and the data are plotted in Fig. 8, together with some of the previously reported parameterizations that have semblance to the functions obtained in our work. Referencing Table 2, for the unstable case, the top sonics at HD and SWA are at z =4 H and $z = 1.5$ H, respectively, and for the stable case, they are at $z = 1.9$ H and $z = 3.2$ H. In both cases, the data from the two sites collapse reasonably well with u_*, pointing to the usefulness of MOST (thus giving credence to underlying assumptions). The present data is closest to Moraes et al. [24], who considered data from above a rice plantation in a valley. All seem to converge to a constant neutral value $\sigma_u/u_* \approx 2.2$, which is similar to that reported in numerous studies [8,56]. Overall, the disparity between the MOST functions in Table 1 points to the non-universality of MOST when applied to the UBL, consistent with the notion of site dependence of G^* in Eq. 5.

3.3.3 Alternative parameterizations for convective turbulence

Alternative parameterizations may be sought for scaling turbulence statistics of the UBL. Table 3 presents parameterizations proposed by André et al. [57] for convective boundary layers (σ_A), Deardorff [58] for oceanic boundary layers (σ_D), and that by Clarke et al. [59] for urban boundary layers (σ_C). They all utilize a composite of mechanical and buoyancy production of turbulence, represented by the friction and convective velocities, respectively.

Figure 9 shows the composite rms velocity $\sigma = \sqrt{TKE}$ scaled by the André et al. [57] parameterization σ_A as a function of the stability parameter ζ for unstable cases; the results for the upper sonic are shown. It appears that σ/σ_A is a constant (≈ 0.8) for unstable cases with an excellent collapse of data. When σ is scaled with σ_D, a collapse similar to that in Fig. 9 was obtained (not shown). A combination of friction and convective velocities appears to be a useful parameterization for convective periods, arguably better than the utility of MOST shown in Fig. 8a. The bane, however, is the necessity of h_u^c in the former.

The Clarke et al. [59] parameterization also produced a good correlation with the rms velocity σ_u (Fig. 10) when plotted for the most vigorous convective period (1230–1700 LST). Here the energy containing wavelength, λ_{max}, was obtained by calculating longitudinal velocity spectrum for 5 min segments, averaging over a total length of 30 min, and locating the wavelength at the spectral peak. Clarke et al. [59] found $C_u \approx$0.4–0.6, but it was noted to be a weak function of urban morphology. The current data has a fit of $C_u \approx 0.68$, which is close to the range previously found, and the variation can be attributed to morphological differences between the cases.

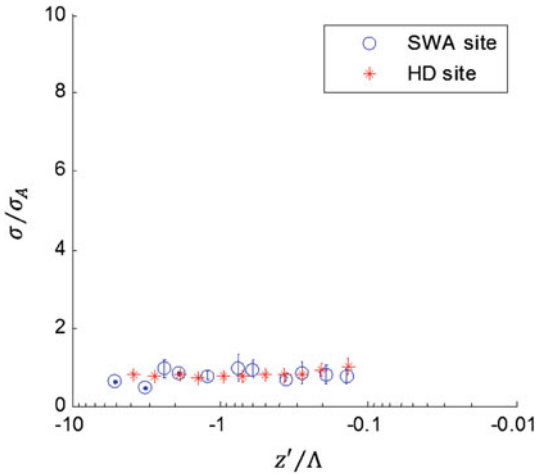

Fig. 9 The composite *rms* velocity normalized by the André et al. [57] velocity scale as a function of stability parameter z'/Λ

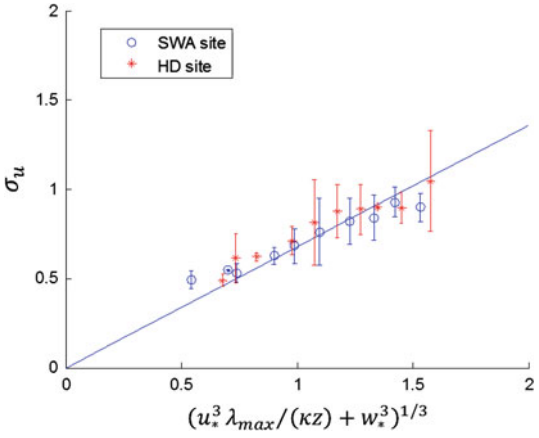

Fig. 10 Thirty minute averages of the u-component of rms velocity against the velocity scale given by Clarke et al. [59]

To summarize, the rms velocities during the convective period are shown in Fig. 11, with normalization by u_*, w_*, σ_A, and σ_C. For consistency, σ has been used in all plots. It is evident that u_* does not collapse the data from the two sites, but w_*, σ_A, (σ_D) and σ_C are better scaling parameters. During strong convective periods, $\sigma = 0.68\sigma_C$, $\sigma = 0.8\sigma_A$, and $\sigma = 0.8\sigma_D$ (not shown) are good representations. Because the performance of σ_A, σ_D, and σ_C are so similar, provided that h_u^c is measured, it may be preferred to use σ_A or σ_D, as they do not require calculation of the spectrum.

3.3.4 Integral length scales

Turbulent length scales are central to evaluating eddy diffusivities of the UBL [40]. The integral scales based on u, v, and w components (L_{uu}^x, L_{vv}^x, L_{ww}^x) of anisotropic turbulence were calculated based on autocorrelation functions, and Taylor's hypothesis [46] was employed to relate temporal measurements to the streamwise spatial coordinate (x); for example, $L_{uu}^x = \bar{u}\int_0^\infty \overline{u'(t)u'(t+\xi)}/\sigma_u^2 d\xi$, where ξ is the time lag with respect to t. Note, however, the limitations of Taylor's hypothesis, which requires $\sigma_u/U < (5\text{–}10)$ %, but naturally for urban flows (σ_u/U) is much larger. The Taylor hypothesis assumes persistence

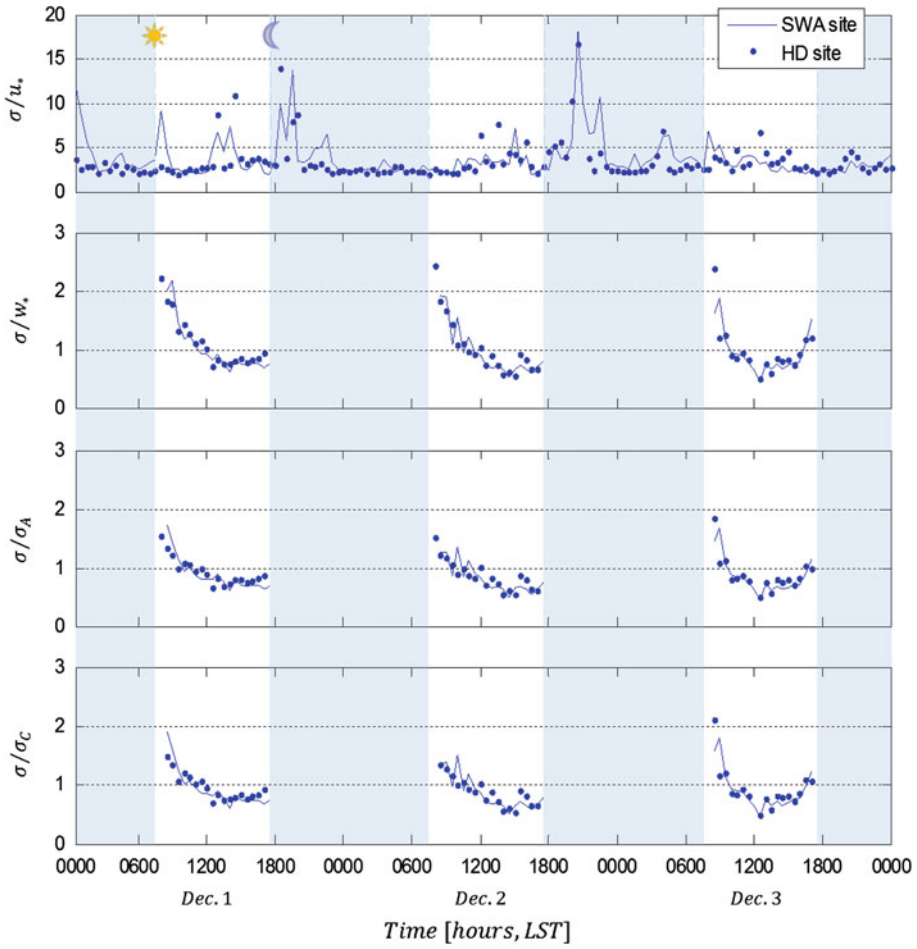

Fig. 11 Thirty minute averages of the normalized composite rms velocity $\sigma = \sqrt{TKE}$ using the different scaling variables as specified in the text on Dec 1–3, 2009 for the two sites

of eddy structures as they sweep past a stationary probe, and only the large structures are expected to behave accordingly at high turbulent intensities; specifically, scales larger than the measurement height may show 'frozen' behavior [60]. For the present case, while L^x_{uu} is mainly contributed to by such low-frequency, large eddies, L^x_{ww} is as much contributed to by smaller eddies of size equal to or smaller than the height of measurement; hence, the latter is more prone to error.

Figure 12 shows the variations of L^x_{uu}, L^x_{vv} and L^x_{ww} with z/H during convective and neutral periods. On physical grounds, one may expect L^x_{uu} and L^x_{vv} to have similarities, but because of the blocking influence of the ground L^x_{ww} is expected to differ, which is evident from Fig. 12. For convenience of interpretation, the expected forms of eddies contributing to the length scales are schematized in Fig. 13, which is a simplified two-dimensional rendition of the UBL of depth h_u.

In sparse canopies, near the ground (typically $z < 0.3h_u$), the w component is dominated by eddies of size $\sim z$, which are (unblocked) isotropic eddies at height z [61]. The horizontal

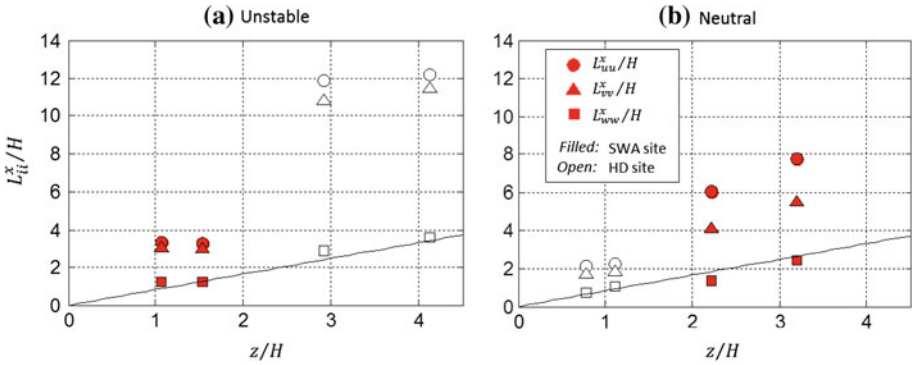

Fig. 12 Variation of the horizontal length scales with the dimensionless height during convective and neutral periods. The line shown is the best fit for the vertical length scales, showing a linear relationship, $L^x_{ww} \approx 0.83z$

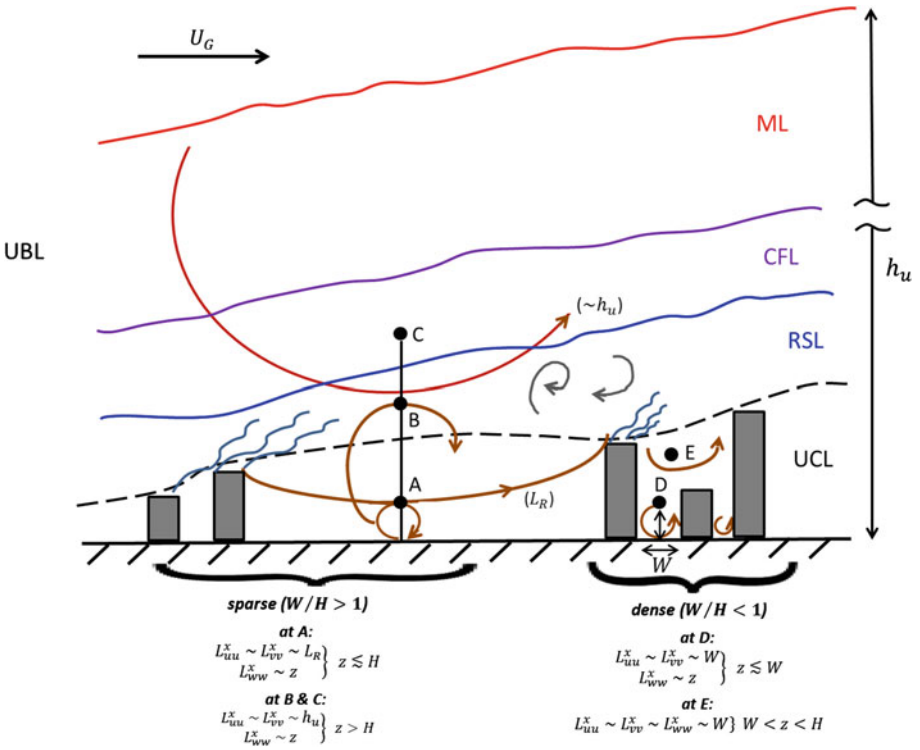

Fig. 13 Proposed schematic of expected forms of integral length scales for the UBL. Definition of acronyms are given in the text

scales, however, are dominated by larger eddies penetrating downward within close proximity of the ground, while being affected by horizontal spacing of the buildings L_R. This is the situation at A within the UCL in Fig. 13. Further up, at B and C, the same applies to the w component, but the horizontal components are less affected by the roughness elements, and hence, scale with h_u.

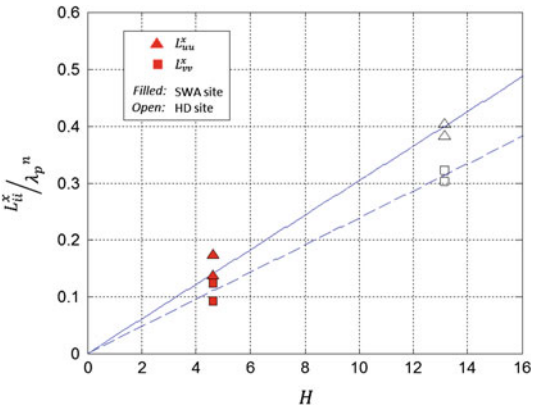

Fig. 14 The variation of L^x_{uu} and L^x_{vv} (normalized by $\lambda_p^{-1.8}$) with H, according to Eq. 12. The *solid line* shows the best fit for L^x_{uu} and the *dotted line* is for L^x_{vv}

On the other hand, within the UCL of *dense canopies*, the width of the urban canyon severely limits the size of eddies. As before, for $z < W$, the *rms* vertical velocity is dominated by isotropic eddies of size $\lesssim z$ whilst the horizontal velocity is dominated by eddies of size $\sim W$. For $z > W$, isotropic motions are determined by recirculating eddies of size $\sim W$, not by $\sim z$, and the length scale W remains important up to $z \sim H$.

The data of Fig. 12 are consistent with the scenario described above for sparse canopies. The L^x_{ww} component increases proportionately to z, $L^x_{ww} \approx 0.83z$. Near the ground, L^x_{uu} and L^x_{vv} are somewhat higher ($\sim L_R$) than L^x_{ww}, but in the RSL and CFL there is a rapid increase of L^x_{uu} and L^x_{vv}, perhaps approaching the order of the UBL thickness h_u. Based on ceilometer measurements during convection $h^c_u \approx 900$ m, and therefore the integral scale above the UCL can be represented as $L^x_{uu} \sim L^x_{vv} \approx (0.03 - 0.06)\, h^c_u$. Fernando et al. [29] argued that for the neutral case in the CFL and upper part of the RSL, the normalized turbulent quantities should be a function of the planar area density λ_p, and in the UCL and RSL, they should additionally depend on parameters such as the frontal area density λ_f and frontal solidarity λ_{fs}. Thus, for the non-neutral case in the CFL and upper RSL, the length scales L^x_{uu} and L^x_{vv} can be represented as

$$\frac{L^x_{uu}}{H} \sim \frac{L^x_{vv}}{H} \sim F\left(\lambda_p, stability\right) \sim \lambda_p^n \Pi\left(stability\right), \tag{12}$$

where the stability of the function Π is specified using an appropriate parameter such as z'/Λ and/or h_u/Λ. Note that L^x_{ww} is excluded, because of its sole dependence on z. Figure 14 shows the dependence of $\left(L^x_{uu}, L^x_{vv}\right)/\lambda_p^n$ on H for data taken in the RSL and CFL (upper two sonics) under neutral conditions, for which Π is a constant; a good agreement with Eq. 12 could be seen for $n = -1.8$, and the best fits are $L^x_{uu}/\lambda_p^n = 3 \times 10^{-2} H$ (solid line in Fig. 14) and $L^x_{vv}/\lambda_p^n = 2.4 \times 10^{-2} H$ (dotted line). Because of the limited availability of data and the dependence on multiple parameters, the stable and unstable cases are not discussed here.

3.4 Nocturnal urban boundary layer

The nocturnal boundary layer is one of the least understood forms of the atmospheric boundary layer [27], and previous studies suggest that either stable or unstable stratification may prevail in urban areas at night. During evening transition, convective turbulence decays, thus lowering the overall turbulent intensity, leaving shear induced (mechanical) turbulence and

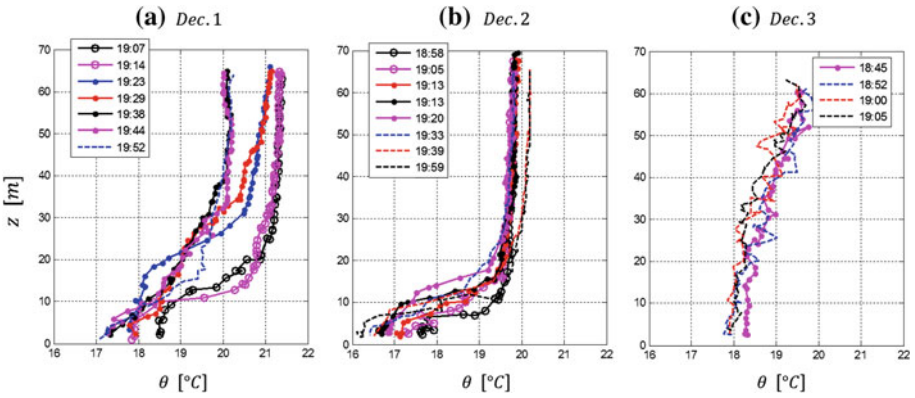

Fig. 15 Individual vertical profiles of potential temperature during the development of stable stratification

UHI as contributors to σ_w. In sparse building canopies the UHI is negligible and when the winds are low, the mechanical turbulence is weak, all providing conditions for stable stratification. This is evident from TKE measurements during the evening transition of Dec 1 and 2 in Fig. 3. The development of stratification, turbulence within this stratified layer, and the height to which ground influence propagates (nocturnal UBL height) are discussed below.

3.4.1 Development of surface stable stratification

The formation of surface stratification in the UBL can be discussed by considering the opposing influences of ground cooling and mechanical turbulence. If the cooling buoyancy flux is $|q_0|$, then a stable layer of thickness δ_s can be generated by a balance between the shear production and (negative) buoyancy flux, $|q_0| \sim \sigma_w^3/\delta_s$, or $\delta_s = c_s\sigma_w^3/|q_0|$; the thickness scale here has similarities to that of MOST but with a different velocity scale. In the oceanic context, Kitaigorodskii [62] proposed $c_s \approx 2$, and Hopfinger and Linden [63] noted, based on laboratory experiments, $c_s \approx 2-7$ (also see the numerical experiments of Noh and Fernando [64]). In urban canopies, for the stable layer to develop in the UCL, $\delta_s < H$, or $c_s < H|q_0|/\sigma_w^3$. In selecting H, it was assumed that if the stratification does not develop near the ground, the possibility of developing it in the lower atmosphere is very low, given enhanced turbulence at the top of the UCL due to shear-layer separation. Note that smaller $|q_0|$ and larger σ_w^3 do not facilitate surface stratification.

Figure 15 shows the balloon profiles for the three design days, for which the magnitudes of $H|q_0|/\sigma_w^3$ are ≈ 5, 2, and 0.2 for Dec 1, 2 and 3 respectively. The development of stable stratification can be clearly seen on Dec 1 and 2, but no indications of such could be seen on Dec 3. Here σ_w and q_0 values were obtained from sonics located in the CFL. Based on those observations, the range for the stable criterion is $c_s \approx 0.2$ (no stratification) to 2 (with stratification). Taken together with the laboratory and oceanic results discussed above, $c_s \approx 2$ is a reasonable value.

3.4.2 Turbulence in the stratified layer

Gibson [65] argued that stratification impedes the growth of turbulence when the vertical inertia forces of energy containing eddies of size L_v (i.e., σ_w^2/L_v) become the same order as their characteristic buoyancy forces (N^2L_v). This yields the limiting vertical length scale

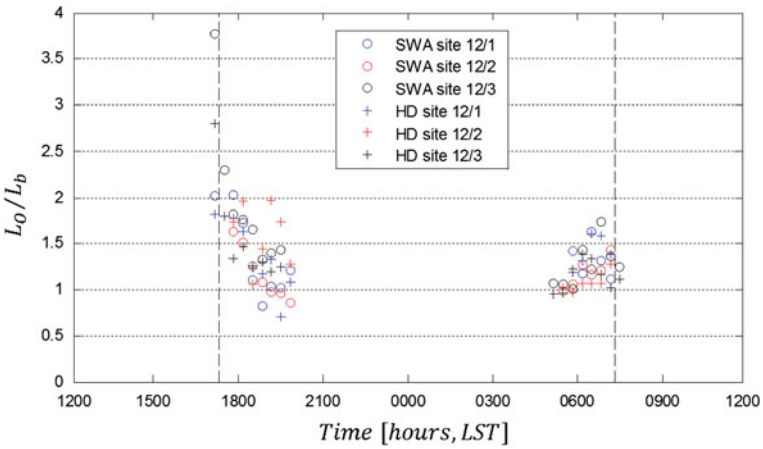

Fig. 16 Daily pattern of the ratio of Ozmidov length scale to buoyancy length scale. Only the upper sonic from each site is shown. (Data shown are during times the balloon was operated)

of stratified turbulence as $L_v \sim L_b$, where $L_b = \sigma_w/N$ is the buoyancy length scale. If the stratification is unimportant, $\sigma_w^2/L_v \gg N^2 L_v$ or $L_v < L_b$. Using the parameterization for high Reynolds number turbulence, $\varepsilon \sim \sigma_w^3/L_v$ [66], the latter condition becomes $L_v < \left(\varepsilon/N^3\right)^{1/2}$, where $L_O = \left(\varepsilon/N^3\right)^{1/2}$ is the Ozmidov scale [65,48]. Thus, at the onset of evening cooling, one may expect $L_O > L_v$ and $L_b > L_v$, but as the turbulence evolves and is affected by stratification, $L_O/L_b \rightarrow constant$. For typical early morning values of $\sigma_w \approx 0.2$m/s and $N \approx 0.02\text{s}^{-1}$, $L_b = \sigma_w/N = 10$m. Laboratory studies show that the thickness of the layer with three-dimensional turbulence is $h_p = 3\sigma_w/N$, when the background gradient Richardson number $Ri_g = N^2/\left(dU/dz\right)^2 > 1$ [49,50]. For $Ri_g < 1$, the three-dimensional turbulent region can propagate much further at the expense of energy derived from shear.

The ratio of L_O/L_b in the CFL is shown in Fig. 16. A clear decreasing trend during the evening transition could be observed, with $L_O/L_b \rightarrow 1.2 \pm 0.2$ after sunset, indicating sustained buoyancy affected turbulence into the night. Even the data on Dec 3, with no surface inversion but with weak stratification aloft, broadly followed this behavior. Since balloon profiles were halted during 2000 to 0500 LST, data for N are missing during this period, but indications are that $L_O/L_b \approx 1.2$ prevails until the early morning. Here ε was evaluated by fitting the Kolmogorov spectral form to the measurements, $E(\kappa) = \alpha_\kappa \varepsilon^{2/3}\kappa^{-5/3}$, with $\alpha_\kappa = 0.5$. The variation of L_O/L_b is consistent with the discussion above on how turbulent eddies are suppressed as stratification evolves [48], contributed to by the decay of convective turbulence due to waning heat flux and the increase of stable density gradient with progressive cooling. Once the stratification sets up, the vertical scale of turbulence near the ground is expected to be the lesser of z and $3L_b$.

3.4.3 Height of the stratified UBL

The stable UBL thickness h_u^s is defined as the height to which the ground influence propagates (Fig. 13). Overall, the outer flow (U_G) at $z > h_u^s$ is driven by large-scale pressure gradients, which is balanced by the ground shear stress (u_*^2), which is transmitted through the UBL. The properties of the stratified UBL depend on external parameters such as the Coriolis parameter

Table 4 Stable boundary layer height parameterizations

Authors	h_u^s	Current data (m)
Pollard et al. [70]	$= 1.7\frac{u_*}{(fN)^{1/2}}$	≈ 170
Zilitinkevich [71], Businger and Arya [72]	$= C\left(\frac{\kappa u_* \Lambda}{f}\right)^{1/2}, C \sim 1$	≈ 200
Yu [73]	$= \left(\frac{1}{30\Lambda} + \frac{f}{0.35u_*}\right)^{-1}$	≈ 450
Nieuwstadt [74]	$= \Lambda\left[\frac{0.3u_*/f\Lambda}{1+1.9h_u^s/L}\right]$	≈ 110
Zilitinkevich et al. [75]	$= 0.4\frac{u_*}{f}\left[1 + \frac{0.4^2 u_*(1+0.25\Lambda N/u_*)}{0.75^2 f\Lambda}\right]^{-1/2}$	≈ 125

f and N, and especially in the upper part of the UBL, f can influence the mean flow and perhaps turbulence. For instance, in the surface layer of intense turbulence (up to the CFL), the Rossby numbers are $u_*/fL_R \sim 10$ and $u_*/fH \sim 200$, and thus, Coriolis effects are unimportant (based on $u_* \sim 0.2$ m/s, $L_R \sim 200$ m, $H \sim 10$ m). In the ML, if $\sigma \sim 0.1$ m/s, the horizontal scale of eddies is $L_H \sim 1$ km, and $f \sim 10^{-4}\text{s}^{-1}$, then $\sigma/fL_H \sim 1$ for turbulence, and for the mean flow, the Rossby number based on mean velocity ~3 m/s and urban length scale ~ 30 km is ~ 1. The baroclinic effects dominate over the urban area for scales $> Nh_u^s/f$, that is over a swath of 40 km or so (for $N \approx 0.02\,\text{s}^{-1}$ and $h_u^s \sim 200$ m). These estimates point to the role of stratified Ekman dynamics above the CFL. Assuming that building morphology is unimportant beyond the RSL, some of the previous work on canonical boundary layers may be applied to the UBL [67].

The simplest is the barotropic case, where the neutral boundary layer depth is $h_u^n = c_1 u_*/f$ [68], and with $c_1 \sim (0.1 - 0.5)$, $h_u^n = (200{-}1{,}000)$ m. When the background flow is stratified, formulations based on integral equations and eddy diffusivity concepts have yielded different expressions for the boundary layer height [69], which are summarized in Table 4, together with estimates based on the current data.

Given the upper limit of our measurement range and the temporal variability of profiles, it was not possible to discern h_u^s using our data. Time averaged profiles with greater height resolution should be able to address this aspect, which is left for future studies.

In some studies, the nocturnal stable boundary layer height h_u^s has been parameterized using $\sigma_w/N \sim u_*/N$ [76,77], which actually represents the region where three-dimensional turbulence and mixing takes place near the ground. The influence of the ground surface, however, propagates much beyond this length scale because of momentum transfer via internal waves and localized turbulence. Therefore, fitting of stable boundary-layer height measurements to $h_u^s = bu_*/N$ may yield highly variable and larger values than expected, and indeed [76,77] reported $b = (4 - 20)$.

4 Conclusions

A field study was conducted in the Hermoso Park neighborhood of Phoenix, Arizona, during Nov 29–Dec 19, 2009, to characterize flow and turbulence in support of air quality investigations mandated by the State Legislature. The study area was made up of industrial/suburban land use and was located in the complex terrain of the Phoenix valley. Two experimental sites (SWA and HD) separated by ≈ 1.5 km were used based on practical needs, and the focus was on days of low synoptic winds conducive for slope and valley winds, and hence, severe air

pollution problems. The up-valley flow was westerly, which switches to down-valley, easterly flow during the night, and thus, approach flow to the sites had different upstream conditions during the day and night. For each site, building morphological parameters z_0, d, λ_p, λ_f, and H were determined using the DEM technique, for easterly and westerly flows. These parameters differ substantially for the different sites, and at a given site for different flow directions.

The flux measurements showed that $z \approx 2H$ may be a reasonable condition for the lower boundary of the CFL, and the applicability of MOST was investigated for $z > 2H$. For neutral stratification, a log-law profile could be detected until the top of the balloon traverse. SODAR data, which extended further, showed that the deviation from the log-law profile occurred at $z \approx 18H$, which can be considered as the top of the CFL.

For the stable UBL, MOST profiles were valid up to $\sim (0.5 - 0.6)\Lambda$ (or for our case $z \sim 6H$), beyond which significant deviations were found. The height of deviations approximately corresponded to the height where turbulent eddies are damped by stratification ($\sim 3L_b$), and hence u_* of the CFL may no longer be representative of local shear stresses. A range of $2H < z < 3L_b$ ($\approx [0.2 - 0.5]\,\Lambda$) is considered to be the CFL for the stable UBL (which means that the CFL may disappear under some conditions). The unstable UBL, as expected, extended to much larger heights, covering the entire measurement height of the balloon, and canonical MOST profiles were in reasonable agreement with observations for $z > 2H$. SODAR data indicated that this agreement may extend as high as $z/H \approx 8$ or $z'/|\Lambda| \approx 2$.

Within the UCL, the velocity profiles were investigated vis-à-vis the theoretical exponential velocity profile suggested in previous work. The agreement was good for unstable and neutral cases, with model constants in broad agreement with those reported in the literature. The agreement for the stably stratified UBL was poor, perhaps because the mixing length model used is questionable in the presence of stable stratification.

Notwithstanding the success of MOST for mean profiles, characterization of turbulence in the CFL appeared to require multiple variables, and hence, any correlation involving z'/Λ alone results in site dependence. Based on similarity arguments, additional variables z_0/Λ and h_u/Λ are expected to play a role. This may explain widely different MOST functions obtained in previous work for turbulent parameters. The present research did not agree with most previous proposals, except for the neutrally stratified case. For the convective case, alternative (hybrid) parameterizations based on a combination of u_* and w_* worked well; simple linear relationships were obtained between turbulent velocities and composite velocity scales. For the nocturnal boundary layer, u_* alone was not the proper scaling variable for rms velocity (data did not collapse).

Calculation of the integral length scales provided useful insights on turbulence in the UBL. For the neutral case, L^x_{uu} and L^x_{vv} were on the order of L^x_{ww} in the UCL, consistent with eddies affected by buildings and constrained within their separation. The horizontal scales are larger within the RSL, but as the effects of buildings wane with the distance from the ground, they grew rapidly to $L^x_{uu} \sim 7.7H$ and $L^x_{vv} \sim 5.5H$ within the CFL. The vertical length scale grew proportionally to z, $L^x_{ww} \approx 0.83$ z, indicating the role of isotropic eddies above the ground in determining vertical motions, while horizontal motions are determined by larger eddies penetrating down from above and distorted by the building canopy. When convection is present, L^x_{ww} was similar to the neutral case, but horizontal length scales in the CFL were larger, perhaps because of a deeper convective boundary layer with larger eddies penetrating downward, facilitated by the sparseness of the building canopy. The convective boundary layer depth h^c_u measured from a ceilometer at a background location indicated $L^x_{uu} \approx (0.03 - 0.06)\, h^c_u$.

A condition for stable stratification in the lower UBL was proposed, $H\,|q_0|\,/\sigma_w^3 > c_s$, where $c_s \approx 2$ was identified. Previous work shows that when turbulence is arrested by buoyancy, certain relationships ought to prevail between specific length scales, in particular, between the Ozmidov scale and buoyancy scale. For the case studied, these relationships were achieved in the evening, and presumably maintained until the morning transition, pointing to quasi-stationary, buoyancy-dominated turbulence in the UBL. This may not be viable for densely built urban canopies that are dominated by the urban heat island phenomenon and/or when the criterion for the development of stratification is not satisfied.

Acknowledgements The experiments described in this paper were funded by the Arizona Department of Environmental Quality as part of the Hermoso Park Study. The data were analyzed with the support of the National Science Foundation CMG Program and the Office of Naval Research Award # N00014-11-1-0709, Mountain Terrain Atmospheric Modeling and Observations (MATERHORN) Program. The authors are grateful to Dr. Laura Leo for assistance in the morphometric analysis and to the students at Arizona State University for their help in setting up the equipment and running balloon flights.

References

1. UNEP. Population Division of the Department of Economic and Social Affairs of United Nations Secretariat (2011) World Population Prospects: The 2010 Revision, Highlights and Advanced Tables.Working Paper ESA/P/WP.220, 142 pp. [Available online at http://www.esa.un.org/unpd/wpp/Documentation/pdf/WPP2010_Highlights.pdf]
2. Fernando HJS, Lee SM, Anderson J, Princevac M, Pardyjak E, Grossman-Clarke S (2001) Urban fluid mechanics: air circulation and contaminant dispersion in cities. Environ Fluid Mech 1:107–164. doi:10.1023/A:1011504001479
3. Li K, Zhang P, Crittenden JC, Guhathakurta S, Chen Y, Fernando HJS, Sawhney A, McCartney P, Grimm N, Kahhat R, Joshi H, Konjevod G, Choi Y-J, Fonseca E, Allenby B, Gerrity D, Torrens PM (2007) Development of a framework for quantifying the environmental impacts of urban development and construction practices. Environ Sci Technol 41:5130–5136. doi:10.1021/es062481d
4. Ching JS, Dupont S, Gilliam R, Burian S, Tang R (2004) Neighborhood scale air quality modeling in Houston using urban canopy parameters in MM5 and CMAQ with improved characterization of mesoscale lake-land breeze circulation. In: Proceeding of 5th Symposium of Urban Environment. Vancouver, August 23–27
5. Settles GS (2006) Fluid mechanics and homeland security. Annu Rev Fluid Mech 38:87–110
6. Andrews MJ, Ginstein FF, Kwicklis E, Linn R (2012) Security and environmental fluid dynamics. In: Fernando HJS (ed) Handbook of environmental fluid dynamics vol 1. CRC Press, Boca Raton, pp 107–121
7. Hang J, Li Y, Sandberg M, Buccolieri R, Di Sabatino S (2012) The influence of building height variability on pollutant dispersion and pedestrian ventilation in idealized high-rise urban areas. Build Environ 56:346–360
8. Britter RE, Hanna SR (2003) Flow and dispersion in urban areas. Annu Rev Fluid Mech 35:469–496. doi:10.1146/annurev.fluid.35.101101.161147
9. Britter RE, Di Sabatino S (2012) Flow through urban canopies. In: Fernando HJS (ed) Handbook of environmental fluid dynamics vol 2. CRC Press, Boca Raton, pp 85–96
10. Oke TR (1988) Boundary layer climates. Routledge, New York
11. Roth M (2000) Review of atmospheric turbulence over cities. Q J R Meteorol Soc 126:941–990
12. Fernando HJS (2010) Fluid dynamics of urban atmospheres in complex Terrain. Annu Rev Fluid Mech 42:365–389
13. Allwine KJ, Shinn JH, Streit GE, Clawson KL, Brown M (2002) Overview of URBAN 2000: A Multiscale Field Study of Dispersion through an Urban Environment. Bull Amer Meteor Soc 83:521–536. http://dx.doi.org.proxy.library.nd.edu/10.1175/1520-0477(2002)083<0521:OOUAMF>2.3.CO;2
14. Allwine KJ, Leach MJ, Stockham LW, Shinn JS, Hosker RP, Bowers JF, Pace JC (2004) Overview of joint urban 2003—an atmospheric dispersion study in Oklahoma City. Bull Am Meteorol Soc 83:745–753
15. Arnold SJ, ApSimon H, Barlow J, Belcher S, Bell M, Boddy JW, Britter R, Cheng H, Clark R, Colvile RN, Dimitroulopoulou S, Dobre A, Greally B, Kaur S, Knights A, Lawton T, Makepeace A, Martin D, Neophytou M, Neville S, Nieuwenhuijsen M, Nickless G, Price C, Robins A, Shallcross D, Simmonds

P, Smalley RJ, Tate J, Tomlin AS, Wang H, Walsh P (2004) Introduction to the DAPPLE air pollution project. Sci Total Environ 332:139–153. doi:10.1016/j.scitotenv.2004.04.020
16. Mestayer PG, Durand P, Augustin P, Bastin S, Bonnefond JM, Bénech B, Campistron B, Coppalle A, Delbarre H, Dousset B, Drobinski P, Druilhet A, Fréjafon E, Grimmond CSB, Groleau D, Irvine M, Kergomard C, Kermadi S, Lagouarde J-P, Lemonsu A, Lohou F, Long N, Masson V, Moppert C, Noilhan J, Offerle B, Oke TR, Pigeon G, Puygrenier V, Roberts S, Rosant J-M, Sanïd F, Salmond J, Talbaut M, Voogt J (2005) The urban boundary-layer field campaign in Marseille (UBL/CLU-ESCOMPTE): set-up and first results. Bound Layer Meteorol 114:315–365
17. Rotach MW, Vogt R, Bernhofer C, Batchvarova E, Christen A, Clappier A, Feddersen B, Gryning S-E, Martucci G, Mayer H, Mitev V, Oke TR, Parlow E, Richner H, Roth M, Roulet Y-A, Ruffieux D, Salmond JA, Schatzmann M, Voogt JA (2005) BUBBLE—an urban boundary layer meteorology project. Theor Appl Climatol 81:231–261
18. Wood CR, Arnold SJ, Balogun AA, Barlow JF, Belcher SE, Britter RE, Cheng H, Dobre A, Lingard JJN, Martin D, Neophytou MK, Petersson FK, Robins AG, Schallcross DE, Smalley RJ, Tate JE, Tomlin AS, White IR (2009) Dispersion experiments in central London: the 2007 DAPPLE project. Bull Am Metrol Soc 90:955–969
19. Barenblatt GI (1996) Scaling, self-similarity, and intermediate asymptotics: dimensional analysis and intermediat asymptotics. Cambridge University Press, Cambridge
20. Brost RA, Wyngaard JC (1978) A model study of the stably stratified planetary boundary layer. J Atmos Sci 35:1427–1440
21. Wood CR, Lacser A, Barlow JF, Padhra A, Belcher SE, Nemitz E, Helfter C, Famulari D, Grimmond CSB (2010) Turbulent flow at 190m height above London during 2006–2008: a climatology and the applicability of similarity theory. Bound Layer Meteorol 137:77–96
22. Panofsky HA, Tennekes H, Lenschow DH, Wyngaard JC (1977) The characteristics of turbulent velocity components in the surface layer under convective conditions. Bound Layer Meteorol 11:355–361
23. Pahlow M, Parlange MB, Porte-Agel F (2001) On Monin-Obukhov similarity in the stable atmospheric boundary layer. Bound Layer Meteorol 99:225–248
24. Moraes OLL, Acevedo OC, Degrazia GA, Anfossi D, da Silva R, Anabor V (2005) Surface layer turbulence parameters over a complex terrain. Atmos Environ 39:3103–3112
25. Wilson JD (2008) Monin-Obukhov functions for standard deviations of velocity. Bound Layer Meteorol 129:353–369
26. Quan L, Hu F (2009) Relationship between turbulent flux and variance in the urban canopy. Meteorol Atmos Phys 104:29–36
27. Fernando HJS, Weil JC (2010) Whither the stable boundary layer? Bull Am Meteorl Soc 91:1475–1484. doi:10.1175/2010BAMS2770.1
28. Grimmond CSB, Salmond JA, Oke TR, Offerle B, Lemonsu A (2004) Flux and turbulence measurements at a densely built-up site in Marseille: heat, mass (water and carbon dioxide), and momentum. J Geophys Res 109:D24101
29. Fernando HJS, Zajic D, Di Sabatino S, Dimitrova R, Hedquist B, Dallman A (2010) Flow, turbulence, and pollutant dispersion in urban atmospheres. Phys Fluids 22:051301–20
30. Pelliccioni A, Monti P, Gariazzo C, Leuzzi G (2012) Some characteristics of the urban boundary layer above Rome, Italy, and applicability of Monin-Obukhov similarity. Environ Fluid Mech, OnlineFirst. doi:10.1007/s10652-012-9246-3
31. Macdonald RW (2000) Modelling the mean velocity profile in the urban canopy layer. Bound Layer Meteorol 97:25–45
32. Kastner-Klein P, Rotach MW (2004) Mean flow and turbulence characteristics in an urban roughness sublayer. Bound Layer Meteorol 111:55–84
33. Baik J-J, Kim J-J, Fernando HJS (2003) A CFD Model for simulating urban flow and dispersion. J Appl Meteorol 42:1636–1648
34. Ellis AW, Hildebrandt ML, Thomas WM, Fernando HJS (2000) Analysis of the climatic mechanisms contributing to the summertime transport of lower atmospheric ozone across metropolitan Phoenix, Arizona, USA. Clim Res 15:13–31
35. Di Sabatino S, Leo LS, Cataldo R, Ratti C, Britter RE (2010) Construction of digital elevation models for a southern european city and a comparative morphological analysis with respect to northern European and North American cities. J Appl Meteorol Climatol 49:1377–1396. doi:10.1175/2010JAMC2117.1
36. Ratti C, Di Sabatino S, Britter RE (2006) Urban texture analysis with image processing techniques: winds and dispersion. Theor Appl Climatol 84:77–90
37. Macdonald RW, Griffiths RF, Hall DJ (1998) A comparison of results from scaled field and wind tunnel modelling of dispersion in arrays of obstacles. Atmos Environ 32:3845–3862

38. Di Sabatino S, Solazzo E, Paradisi P, Britter R (2008) A simple model for spatially-averaged wind profiles within and above an urban canopy. Bound Layer Meteorol 127:131–151
39. Grimmond CSB, Oke TR (1999) Aerodynamic properties of urban areas derived from analysis of surface form. J Appl Meteorol 38:1262–1292
40. Belcher SE, Jerram N, Hunt JCR (2003) Adjustment of a turbulent boundary layer to a canopy of roughness elements. J Fluid Mech 488:369–398. doi:10.1017/S0022112003005019
41. Lenschow DH, Mann J, Kristensen L (1994) How long is long enough when measuring fluxes and other turbulence statistics? J Atmos Ocean Technol 11:661–673
42. Brazel AJ, Fernando HJS, Hunt JCR, Selover N, Hedquist BC, Pardyjak E (2005) Evening transition observations in Phoenix, Arizona. J Appl Meteorol 44:99–112
43. Hunt JCR, Fernando HJS, Princevac M (2003) Unsteady thermally driven flows on gentle slopes. J Atmos Sci 60:2169–2182
44. Lee S-M, Fernando HJS, Princevac M, Zajic D, Sinesi M, McCulley JL, Anderson J (2003) Transport and diffusion of ozone in the nocturnal and morning planetary boundary layer of the Phoenix valley. Environ Fluid Mech 3:331–362
45. Fernando HJS, Verhoef B, Di Sabatino S, Leo LS, Park S (2013) The Phoenix evening transition flow experiment (TRANSFLEX). Bound Layer Meteorol. doi:10.1007/s10546-012-9795-5
46. Kaimal JC, Finnigan JJ (1994) Atmospheric boundary layer flows: their structure and measurement. Oxford University Press, Oxford
47. Wang Y, Klipp CL, Garvey DM, Ligon DA, Williamson CC, Chang SS (2007) Nocturnal low-level-jet-dominated atmospheric boundary layer observed by a doppler lidar over Oklahoma City during JU2003. J Appl Meteorol Clim 46:2098–2109
48. Gibson CH (1991) Laboratory, numerical, and oceanic fossil turbulence in rotating and stratified flows. J Geophys Res 96:12549–12566
49. Fernando HJS (2003) Turbulent patches in stratified shear flows. Phys Fluids 15:3164–3169
50. Fernando HJS (2005) Turbulent patches in a stratified shear flow. Phys Fluids 17:078102
51. De Silva IPD, Fernando HJS (1992) Some aspects of mixing in a stratified turbulent patch. J Fluid Mech 240:601–625
52. Cionco RM (1965) A mathematical model for air flow in a vegetative canopy. J Appl Meteorol 4:517–522
53. Karlsson S (1986) The applicability of wind profile formulas to an urban-rural interface site. Bound Layer Meteorol 34:333–355
54. Pérez IA, García MA, Sánchez ML, de Torre B (2005) Analysis and parameterization of wind profiles in the low atmosphere. Sol Energy 78:809–821
55. Hicks BB, Callahan WJ, Dobosy RJ, Novakovskaia E (2012) Urban turbulence in space and in time. J Appl Meterol Clim 51:205–218
56. Hanna SR, Britter RE (2002) Wind flow and vapor cloud dispersion at industrial sites. Am. Inst. Chem Eng, New York
57. André JC, De Moor G, Lacarrere P, Therry G, Du Vachat R (1978) Modeling the 24-hour evolution of the mean and turbulent structures of the planetary boundary layer. J Atmos Sci 35:1861–1883
58. Deardorff JW (1983) A multi-limit mixed-layer entrainment formulation. J Phys Oceanogr 13:988–1002
59. Clarke JF, Ching JKS, Godowitch JM (1982) An experimental study of turbulence in an urban environment. Technical Report US EPA, Research Triangle Park. NMS PB 226085
60. Higgins CW, Froidevaux M, Simeonov V, Vercauteren N, Barry C, Parlange MB (2012) The effect of scale on the applicability of Taylor's Frozen turbulence hypothesis in the atmospheric boundary layer. Bound Layer Meteorol 143:379–391
61. Hunt JCR (1984) Turbulence structure in thermal convection and shear-free boundary layers. J Fluid Mech 138:161–184
62. Kitaigorodskii SA (1960) On the computation of the thickness of the wind-mixing layer in the ocean. Bull Acad Sci USSR Geophys Ser 3:284–287
63. Hopfinger EJ, Linden PF (1982) Formation of thermoclines in zero-mean-shear turbulence subjected to a stabilizing buoyancy flux. J Fluid Mech 114:157–173
64. Noh Y, Fernando HJS (1991) A numerical study on the formation of a thermocline in shear-free turbulence. Phys Fluids A 3:422–426
65. Gibson CH (1982) Alternative interpretations for microstructure patches in the thermocline. J Phys Oceanogr 12:374–383
66. Batchelor GK (1967) An introduction to fluid dynamics. Cambridge University Press, Cambridge
67. Dobbins RA (1977) Observations of the barotropic Ekman layer over an urban terrain. Bound Layer Meteorol 11:39–54
68. Rossby CG, Montgomery RB (1935) The layer of frictional influence in wind and ocean currents. Pap Phys Oceanogr Meteorol 3:1–101

69. Vickers D, Mahrt L (2004) Evaluating formulations of stable boundary layer height. J Appl Meteorol 43:1736–1749
70. Pollard RT, Rhines PB, Thompson RORY (1973) The deepening of the wind-mixed layer (in the ocean). Geophys Fluid Dyn 4:381–404
71. Zilitinkevich S (1972) On the determination of the height of the Ekman boundary layer. Bound Layer Meteorol 3:141–145
72. Businger JA, Arya SPS (1975) Heights of the mixed layer in the stably stratified planetary boundary layer. In: Frenkiel FN, Munn RE (eds) Advances in geophysics vol 18A. Elsevier, Engelska, pp 73–92
73. Yu TW (1978) Determing the height of the nocturnal boundary layer. J Appl Meteorol 17:28–33
74. Nieuwstadt FTM (1981) The steady-state height and resistance laws of the nocturnal boundary layer: theory compared with Cabauw observations. Bound Layer Meteorol 20:3–17
75. Zilitinkevich S, Baklanov A, Rost J, Smedman AS, Lykosov V, Calanca P (2002) Diagnostic and prognostic equations for the depth of the stably stratified Ekman boundary layer. Quart J Roy Meteorol Soc 128:25–46
76. Kitaigorodskii SA (1988) A note on similarity theory for atmospheric boundary layers in the presence of background stable stratification. Tellus 40A:434–438
77. Kitaigorodskii SA, Joffre SM (1988) In search of simple scaling for the heights of the stratified atmospheric boundary layer. Tellus 40A:419–433